Supporting Information

Revealing the Role of Bridging Oxygen in Carbon Shell Coated Ni Interface for Enhanced Alkaline Hydrogen Oxidation Reaction

Pengyu Han,[†a] Xinyi Yang,[†a] Liqing Wu,[†a] Hongnan Jia,[a] and Wei Luo*[a]

[a]College of Chemistry and Molecular Sciences, Wuhan University, Wuhan, Hubei 430072, P. R. China.

*Corresponding author. E-mail addresses: wluo@whu.edu.cn.

[†]These authors are contributed equally to this work.

Experimental Procedures

Chemicals

All chemicals were used as received without any further purification. Nickel nitrate hexahydrate ($Ni(NO_3)_2 \cdot 6H_2O$, 98%, Sinopharm Chemical Reagent Co., Ltd.), terephthalic acid (H_2BDC, 99%, Sinopharm Chemical Reagent Co., Ltd.), 4-Carboxyphenylboronic acid ($C_7H_7BO_4$, 97%, Macklin Corporation), N, N-Dimethylformamide (DMF, 99.5%, Sinopharm Chemical Reagent Co., Ltd.), ethanol (C_2H_5OH, 99.7%, Sinopharm Chemical Reagent Co., Ltd.), nickel oxide (NiO, 99.5%, Bide Pharmatech Ltd.), nickel sulfate hexahydrate ($NiSO_4 \cdot 6H_2O$, 98.5%, Linfeng Chemical Reagent (Shanghai) Co., Ltd.), sodium borohydride ($NaBH_4$, 97%, Linfeng Chemical Reagent (Shanghai) Co., Ltd.), potassium hydroxide (KOH, 99.99% metals basis, except sodium, Aladdin Industrual Co. Ltd.), isopropyl alcohol (C_3H_8O, 99.7%, Sinopharm Chemical Reagent Co. Ltd.), Nafion solution (5 wt%, Sigma-Aldrich Co. Ltd.), commercial Pt/C (20%, Johnson Matthey Hispec 3600, Shanghai Hesen Electric). Support: carbon black (Vulcan, XC-72R). The ultrapure water (18.25 MΩ cm^{-1}) was used throughout the whole experiment.

Synthesis of Ni-BDC

In a typical synthesis, 930.5mg $Ni(NO_3)_2 \cdot 6H_2O$ and 498.4 mg H_2BDC were added into 30 mL DMF and the mixtures were ultrasonicated for 10 minutes to completely dissolve. Then, 2.5 mL ethanol and 2.5 mL ultrapure water were added into the solution and ultrasonicated for another 5 minutes. After that, the solution was transferred to a 50 mL

Teflon-lined stainless-steel autoclave and kept at 120 ℃ for 12h. After cooling down to room temperature, the precipitate was collected by centrifugation and washed with DMF and ethanol for three times, then dried in a vacuum drier overnight at room temperature.

Synthesis of Ni-BDC-BA

The synthesis of Ni-BDC-BA was the same as that of Ni-BDC, except that the H_2BDC was partial replaced by 4-carboxylphenylboronic acid in the first step, and their feeding molar ratio are 8:2, 5:5 and 2:8 (H_2BDC: 4-carboxylphenylboronic acid), respectively. Finally, the precipitates were denoted as Ni-BDC-BA 8:2, Ni-BDC-BA 5:5 and Ni-BDC-BA 2:8.

Synthesis of Ni@C and Ni@BC

Typically, the obtained Ni-BDC or Ni-BDC-BA powder was put into the quartz boat and placed in the center of the tube furnace to prepare Ni@C and Ni@BC catalysts, respectively. The furnace was purged with mixture of gases (95% N_2 and 5% H_2), and then heated to 400 °C with a ramp rate of 2 °C min^{-1}. After reacting 2 h, the furnace was cooled down to room temperature naturally and the precipitate was collected. The obtained products were denoted as Ni@C, Ni@BC 8:2, Ni@BC 5:5 and Ni@BC 2:8, respectively. In this article, the obtained Ni@BC 5:5 was employed as the best sample to compare with Ni@C and Ni, and was marked Ni@BC in the text.

Synthesis of Ni

To pure Ni catalyst was prepared by a modified previous method,[1] 263 mg $NiSO_4 \cdot 6H_2O$ was dissolved in 10 mL water under stirring and ice-bath, then 10 mL water solution containing 96 mg $NaBH_4$ was added dropwise into the $NiSO_4$ solution. After reacting for 3h, the mixture was transferred into a 100 mL autoclave and held at 150 °C for 6h. When the autoclave was cooled down to room temperature, the precipitate was collected by centrifugation and washed with water and ethanol, then dried in a vacuum drier. At last, the dried precipitate was annealed at 300 °C for 1 h under N_2/H_2 atmosphere, and the obtained sample was denoted as Ni.

Physical characterization

The X-ray powder diffraction (XRD) patterns were performed on a Rigaku Miniflex600 X-ray powder diffractometer equipped with a Cu Kα radiation source (λ = 0.154178 nm). All the diffraction data were collected in a 2θ range from 10° to 80° at a scanning rate of 10° min^{-1}. The transmission electron microscopy (TEM) observation was performed using a JEM-2100Plus operated at 200 kV. The high-resolution TEM (HRTEM) images and the energy dispersive spectroscopy (EDS) data were obtained on a Tecnai G2 F30 transmission electron microscope equipped with an EDX spectrometer at an acceleration voltage of 300 kV. The X-ray photoelectron spectroscopy (XPS) measurement was conducted in a Thermo Fischer ESCALAB 250Xi spectrophotometer. The X-ray absorption fine structure spectra of Ni K-edge were carried out using Deep Inspectra in situ XAFS spectroscopy system (Beijing Scistar Technology Co. Ltd). The

C K-edge XANES spectra were collected in Beamlines MCD-A and MCD-B (Soochow Beamline for Energy Materials) at NSRL. Inductively coupled plasma atomic emission spectroscopy (ICP-AES) was performed on a Thermo IRIS Intrepid II XSP atomic emission spectrometer. Zeta potential measurements were carried out using Zeta sizer NanoZS ZEN3600 device by Malvern Instruments. The solutions for Zeta potential tests were prepared by dissolving catalysts into ultrapure water.

Preparation of working electrodes

The working electrode was prepared as followed: 4 mg sample and 1 mg XC-72 were dispersed in 1.0 mL solvent of isopropyl alcohol containing 0.05 wt.% Nafion and then ultrasonicated for at least 30 min to form a homogeneous ink. The glassy-carbon electrode (GCE, 5 mm in diameter) was polished with 0.05 μm alumina powder successively to obtain a mirrorlike surface, and then washed with ultrapure water and ethanol with sonication to obtain a neat surface. After the GCE was dried in air, 12 μL of the ink was drop-casted on the surface of the GCE intermittently and dried in air before any electrochemical measurements. The loadings of Ni on electrocatalysts decorated electrodes could be calculated from the ICP-AES data (Table S2).

Electrochemical Measurements

Electrochemical measurements were performed on a CHI 760E electrochemical analyzer (CH Instruments, Chenhua Co., Ltd.) in a conventional one-component three-electrode cell by using the modified GCE with various catalyst samples as the working

electrodes, a Hg/HgO electrode (full filled with 0.1 M KOH) as the reference electrode and the graphite rod (diameter of 5 mm) as the counter electrode. In this work, all the measured potentials were referred to the reversible hydrogen electrode (RHE) potential. For each electrochemical test, fresh 0.1 M potassium hydroxide (KOH) solution was employed as the electrolyte. Before hydrogen oxidation reaction (HOR) evaluation, we stabilized the GC disk surface at open circuit potential for more than 300 s in H_2-saturated 0.1 M KOH solution. Then, the polarization curves were recorded by a rotating disk electrode (RDE) system (Pine Research Instruments) with the rotation rate of 2500 revolutions per minute (rpm). The potential was scanned from -0.08 V to 0.12 V (vs. RHE) at a scan rate of 5 mV s^{-1}.

Electrochemically active surface areas (ECSAs) were determined by cyclic voltammetry that conducted in 0.1 M KOH solution with Ar-saturated at a scanning rate of 50 mV s^{-1} from -0.18 V to 0.52 V. The value of ECSA (cm_{metal}) can be calculated via Eq. S1,[1]

$$ECSA = \frac{Q_{Ni}}{Q_S} \qquad \text{Eq. S1}$$

where Q_{Ni} is the measured integral charge that corresponds the area of the shaded area, Q_s is the surface charge density of 514 μC cm_{Ni}^{-2}, which is assumed for one monolayer of OH adsorption on Ni.

Electrochemical impedance spectra (EIS) tests were carried out after each RDE measurement with the AC impedance spectra from 200 kHz to 0.1 kHz and a voltage perturbation of 5 mV. The real part of the resistance at 1 kHz was taken as the

uncompensated resistance (R_u) and was used to obtain the *iR*-free potential ($E_{iR\text{-free}}$) according to the following equation, Eq. S2,[2]

$$E_{iR-free} = E - iR_u \quad \text{Eq. S2}$$

where E is the measured potential and i is the corresponding current.

Kinetic current density (j^k) could be extracted from the Koutecky–Levich equation (Eq. S3),

$$\frac{1}{j} = \frac{1}{j^k} + \frac{1}{j^d} = \frac{1}{j^k} + \frac{1}{BC_0\omega^{1/2}} \quad \text{Eq. S3}$$

where j, j^d, B, c_0, and ω are the measured current density, the diffusion limited current density, the Levich constant, the solubility of H_2 (7.33×10^{-4} mol L^{-1}), and the speed of the rotating speed, respectively.[2] Among them, B could be calculated from Eq. S4,

$$B = 0.2nFD^{2/3}\nu^{-1/6} \quad \text{Eq. S4}$$

where n, F, D, and ν are the number of electrons transferred (2), the Faraday constant (96485 C mol^{-1}), the diffusivity of H_2 (3.7×10^{-5} cm^2 s^{-1}), and the kinematic viscosity (1.01×10^{-2} cm^2 s^{-1}), respectively.[2]

Exchange current density (j^0), often used to evaluate the intrinsic activity of a catalyst, could be deduced from the Butler–Volmer equation (Eq. S5),

$$j^k = j^0[e^{\frac{\alpha F}{RT}\eta} - e^{\frac{-(1-\alpha)F}{RT}\eta}] \quad \text{Eq. S5}$$

where α, R, T, and η represent the transfer coefficient, the universal gas constant (8.314 J mol^{-1} K^{-1}), the operating temperature (303 K in this work), and the overpotential, respectively.[3]

j^0 could be also obtained from the approximate Butler-Volmer equation (Eq. S6),[3]

$$j = j^0\frac{\eta F}{RT} \quad \text{Eq. S6}$$

CO-tolerance test was performed using the same electrochemical measurements of HOR test. The working electrode were prepared by 5 μL of 20 wt% Pt/C ink dropping onto the RDE electrode to achieve catalyst loading of 10 μg_{Pt} cm^{-2} (Ni@BC keep the same loading as the former test). The long-term stability tests were performed using chronoamperometry conducted in 0.1 M KOH saturated with CO containing (100 ppm) hydrogen at the rotating speed of 2500 rpm (1600 rpm for Pt/C) and measured at 0.05 V for more than 1 h.

The stability of Ni@BC catalyst was evaluated by the accelerated durability tests in hydrogen and Ar-saturated solutions for 1000 cycles at the scanning rate of 0.5 V s^{-1} by scanning the potential between -0.05 to 0.12 V and -0.08 to 0.42 V, respectively.

To perform CO stripping test, the electrode was firstly held at constant potential (0.1 V vs RHE) for ten minutes in the purged carbon monoxide to adsorb CO on the metal surface. Then, Ar was purging for about 20 min to exclude residual CO in 0.1 mol L^{-1} KOH. Finally, the cyclic voltammetry curve of CO stripping was recorded in a potential window between 0 to 1.2 V at a sweep rate of 10 mV s^{-1}.

For HER testing, 4 mg catalyst and 1 mL XC-72 carbon support were mixed with 1 mL solvent of isopropyl alcohol containing 0.1 wt.% Nafion and ultrasonicated to form a homogeneous ink. After that, 12 μL ink was drop-casted on the surface of the GCE and dried in air before electrochemical measurements. For commercial Pt/C, the working electrode was prepared by dropping 6 μL of 20 wt% Pt/C ink onto the RDE electrode to achieve catalyst loading of 30 μg_{Pt} cm^{-2}. Then, the HER tests were performed in Ar-saturated 1 M KOH at 5 mV s^{-1} with the rotating speed of 1600 rpm.

Density functional theory (DFT) calculations

All the DFT calculations applied in this paper were performed by using CASTEP code of the Materials Studio package of Accelrys Inc. The electron interactions were described using the Perdew-Burke-Ernzerhof (PBE) exchange correlation functional within the generalized gradient approximation (GGA) scheme.[4] The interaction between valence electrons and ionic cores was described by Ultrasoft pseudopotential.[5] For geometric optimizations, the smearing method of Methfessel-Paxton (MP) and smearing widths of 0.1 eV were applied.[6] The cutoff energy was 400 eV and the self-consistent field (SCF) tolerance was 1×10^{-6} eV. The Brillouin zone was sampled using the Monkhorst Pack method, and the number of k points was set according to the model, of which 4×4×1 was set for all the geometric optimization. We choose Ni (111) face as the model of Ni metal catalyst for calculation. By coating a layer C atom on the top of Ni (111) face through O atoms with B doping C or not, the Ni@BC and Ni@C catalysts models were established. For all calculations, the atoms in the bottom layer were fixed in the equilibrium positions, while the rest of the atoms were fully relaxed. The thickness of vacuum layer along the z-direction is set as 15 Å to separate the upper and lower surfaces. The adsorption free energies of various intermediates (e.g., H*, OH*) on a certain surface is calculated by $\Delta G = \Delta E + \Delta ZPE - T\Delta S$, where ΔE is the DFT based adsorption energy of intermediate, ΔZPE and $T\Delta S$ are the correction of zero point energy and entropy, respectively. The relative entropies and zero point energies (ZPEs) of various species are from previous reports.[7,8]

Results and Discussion

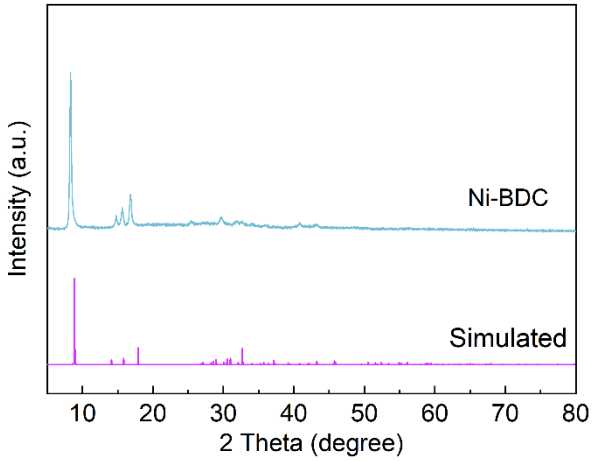

Figure S1. XRD patterns of the synthesized Ni-BDC.

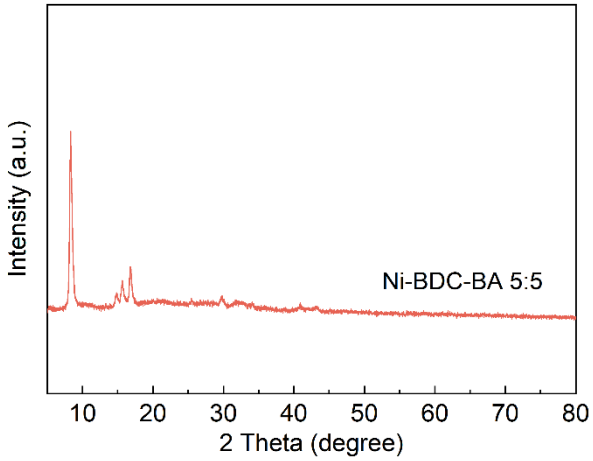

Figure S2. XRD patterns of the synthesized Ni-BDC-BA 5:5.

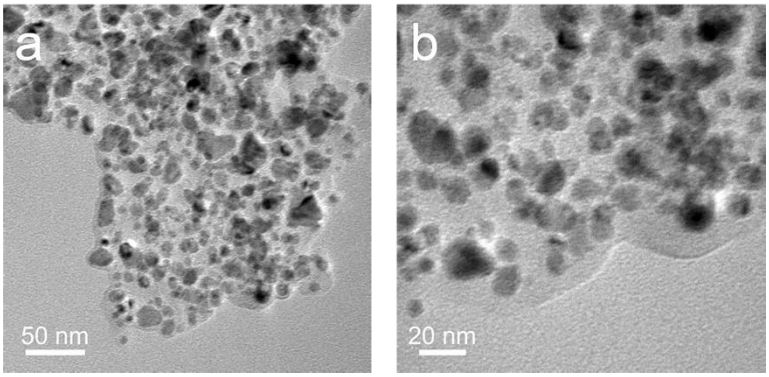

Figure S3. TEM images of Ni@C.

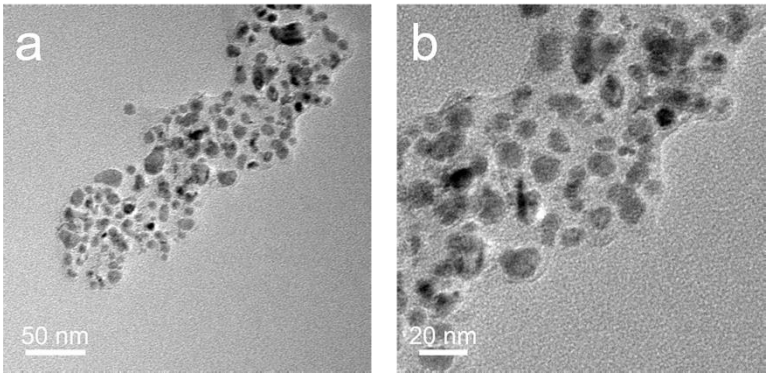

Figure S4. TEM images of Ni@BC derived from the pyrolysis of Ni-BDC-BA 5:5.

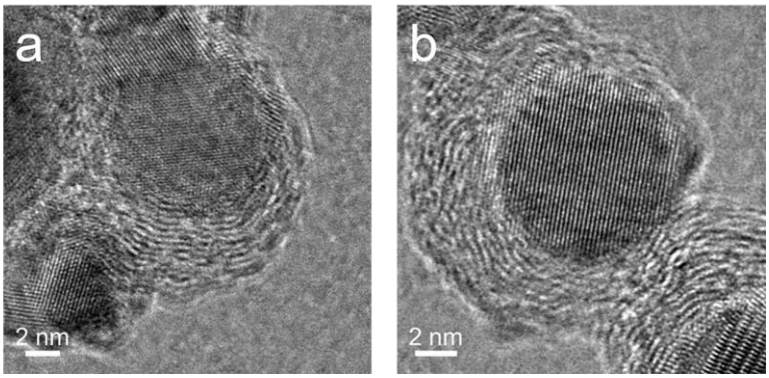

Figure S5. High-resolution TEM (HRTEM) images of Ni@BC.

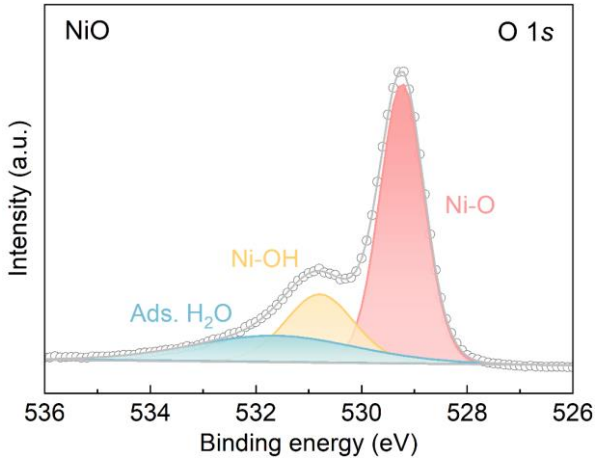

Figure S6. High-resolution XPS spectra of O 1s in NiO.

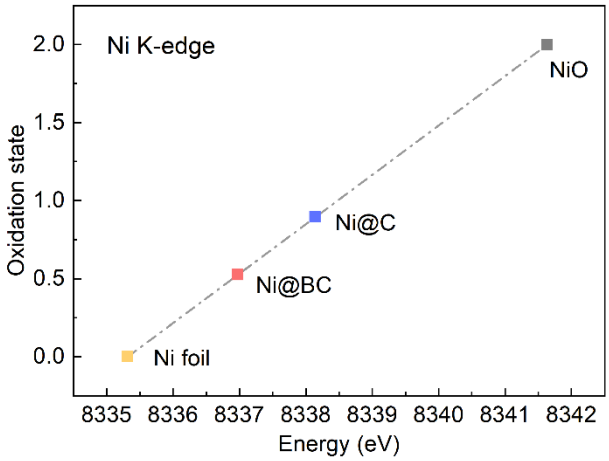

Figure S7. Average oxidation states of Ni calculated from the XANES spectra of samples.

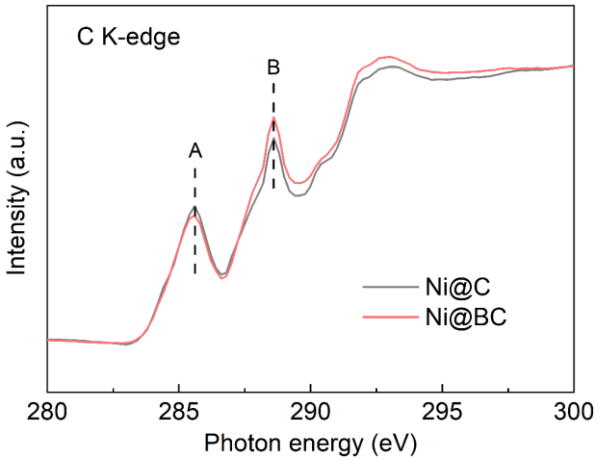

Figure S8. The C K-edge X-ray absorption near edge structure (XANES) spectra of Ni@C and Ni@BC.

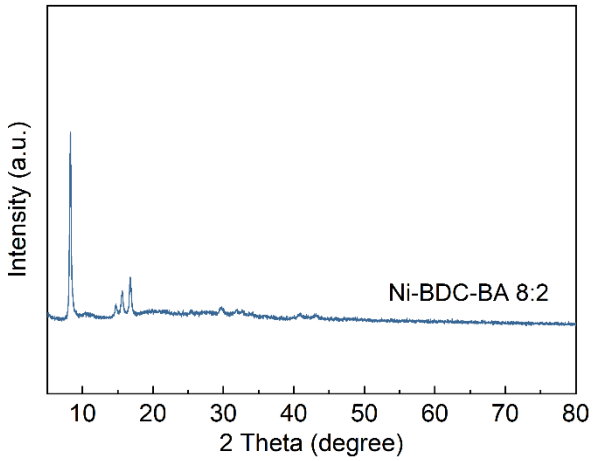

Figure S9. XRD patterns of the synthesized Ni-BDC-BA 8:2.

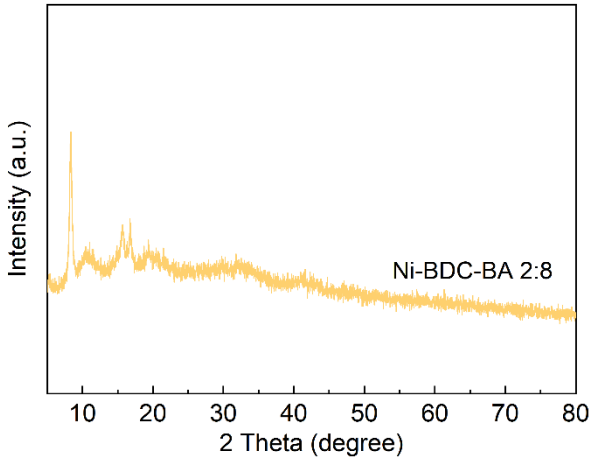

Figure S10. XRD patterns of the synthesized Ni-BDC-BA 2:8.

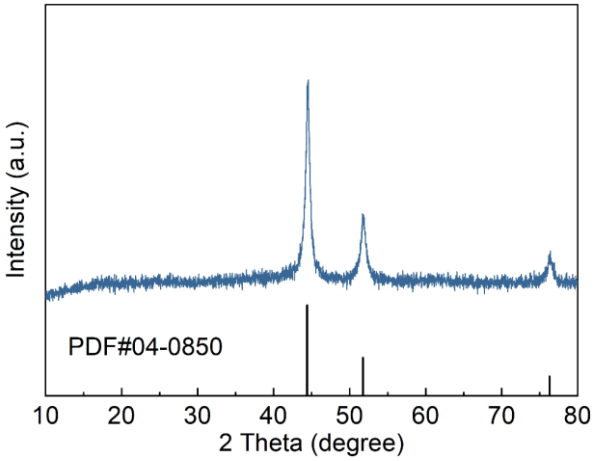

Figure S11. XRD patterns of Ni@BC 8:2.

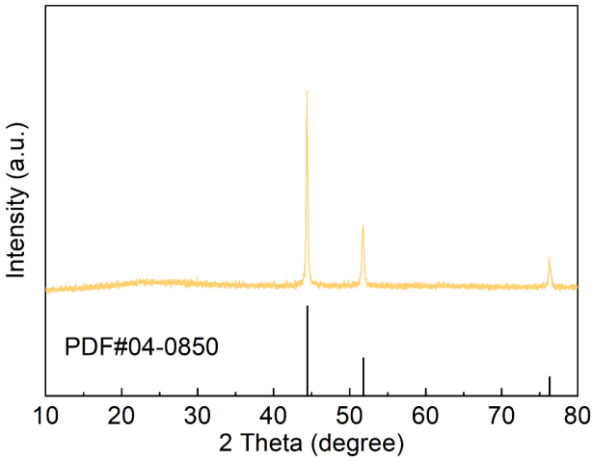

Figure S12. XRD patterns of Ni@BC 2:8.

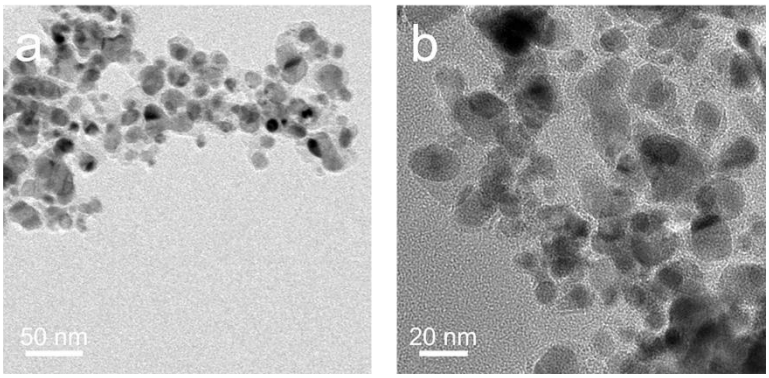

Figure S13. TEM images of Ni@BC 8:2.

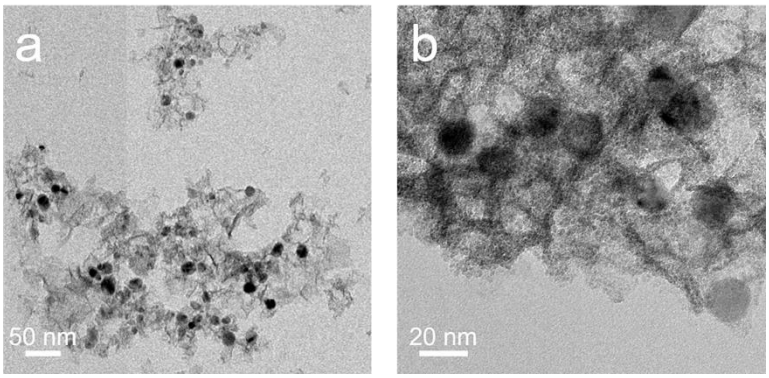

Figure S14. TEM images of Ni@BC 2:8.

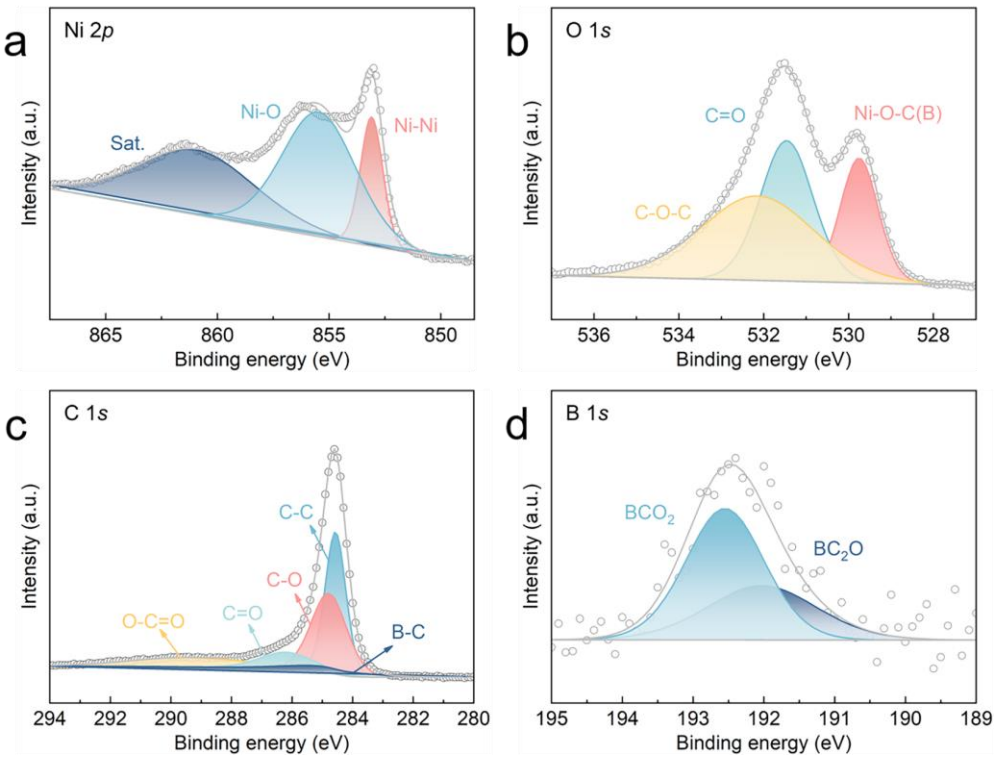

Figure S15. High-resolution XPS spectra of (a) Ni 2*p*, (b) O 1*s*, (c) C 1*s* and (d) B 1*s* in Ni@BC 8:2.

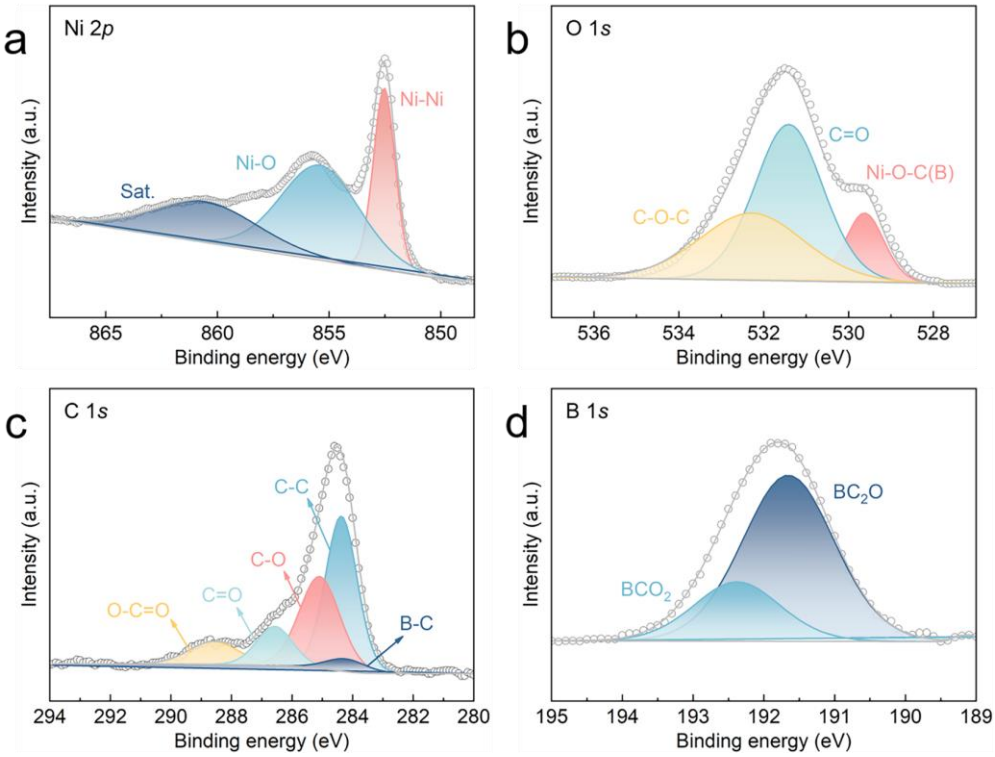

Figure S16. High-resolution XPS spectra of (a) Ni 2*p*, (b) O 1*s*, (c) C 1*s* and (d) B 1*s* in Ni@BC 2:8.

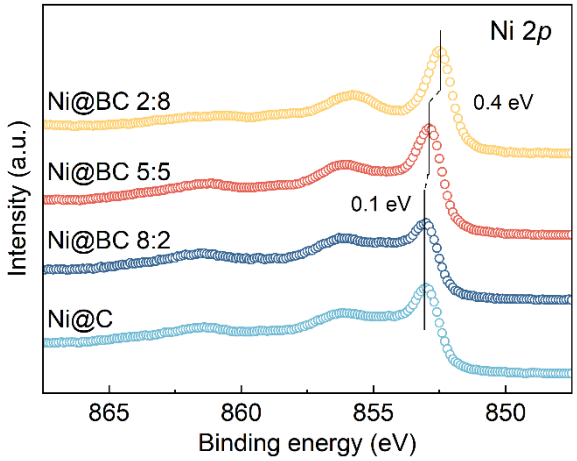

Figure S17. High-resolution XPS spectra of Ni 2*p* in Ni@C, Ni@BC 8:2, Ni@BC 5:5 and Ni@BC 2:8.

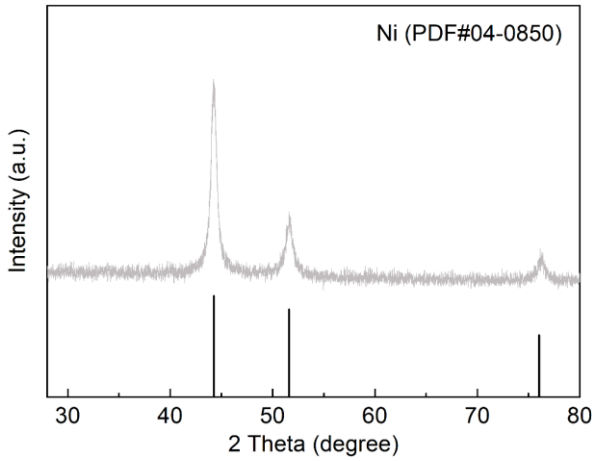

Figure S18. The XRD patterns of synthesized pure Ni.

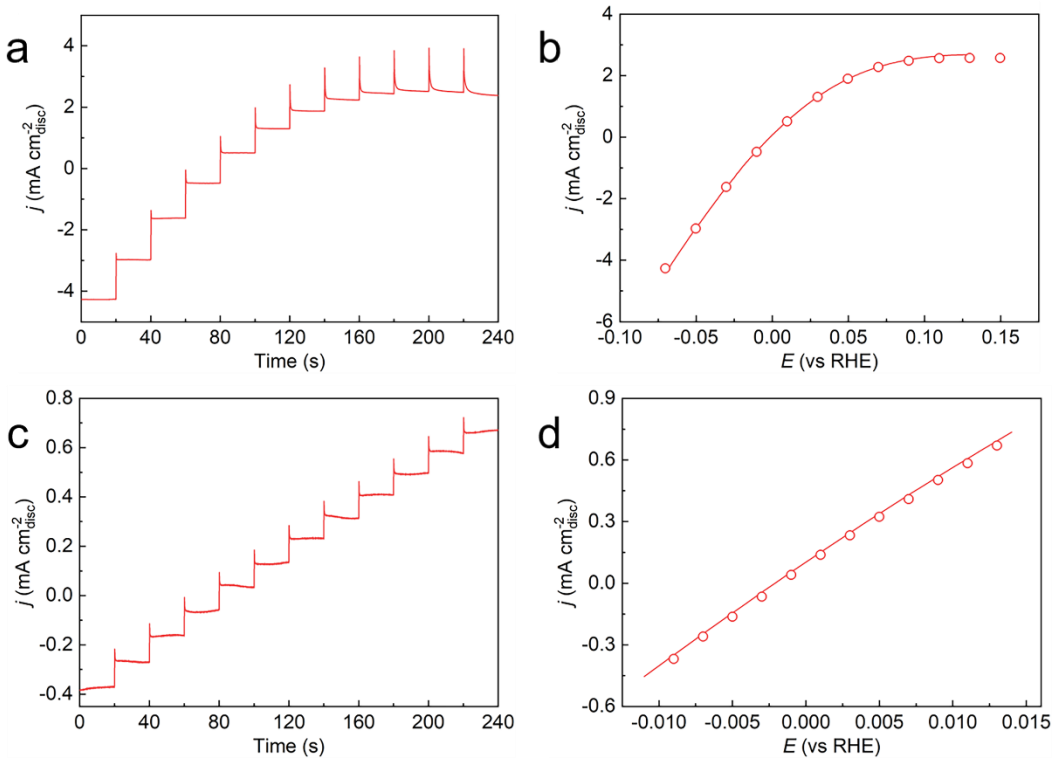

Figure S19. Electrochemical activity measurements of Ni@BC in H_2-saturated 0.1 M KOH at 2500 rpm. (a) Current density vs. time response of Ni@BC to the potential program applied with the potential step of 20 mV. (b) Steady-state polarization curve (circle) and the corresponding transient polarization curve (line) obtained by LSV. (c) Current density vs. time response of Ni@BC to the potential program applied with the potential step of 2 mV. (d) Steady-state polarization curve (circle) and the corresponding transient polarization curve (line) obtained by LSV at the micropolarization regions. The potentials were not *iR* corrected.

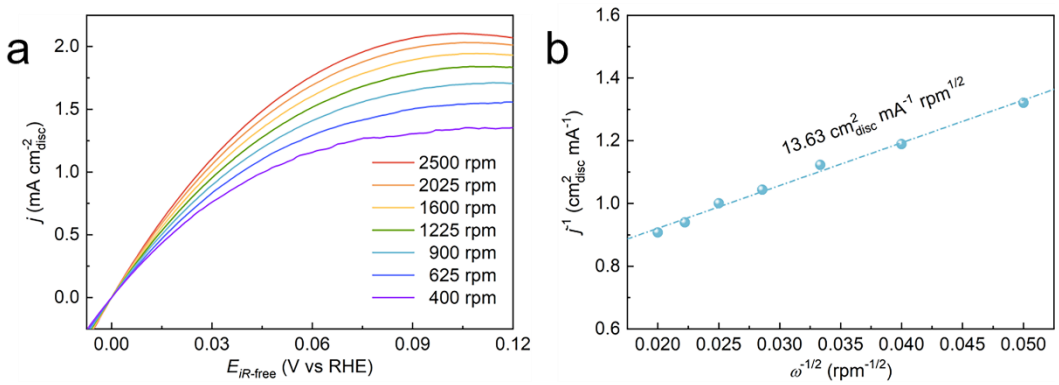

Figure S20. (a) HOR polarization curves of Ni@C in H_2-saturated 0.1 M KOH with a scan rate of 5 mV s^{-1} at the rotating speeds varied from 2500 to 400 rpm. (b) Koutecky–Levich plot obtained from (a) at an overpotential of 30 mV.

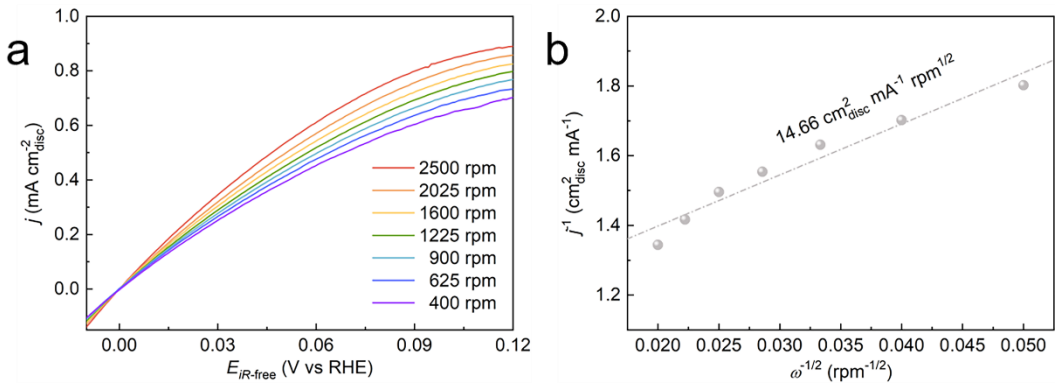

Figure S21. (a) HOR polarization curves of Ni in H_2-saturated 0.1 M KOH with a scan rate of 5 mV s^{-1} at the rotating speeds varied from 2500 to 400 rpm. (b) Koutecky–Levich plot obtained from (a) at an overpotential of 80 mV.

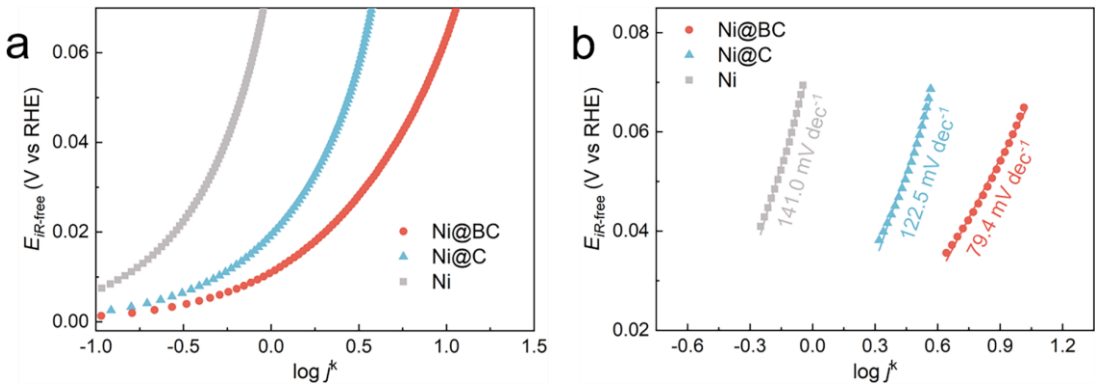

Figure S22. (a) Tafel plots of HOR branch, (b) Tafel slopes of HOR branch for Ni, Ni@C and Ni@BC in H_2-saturated 0.1 M KOH solution.

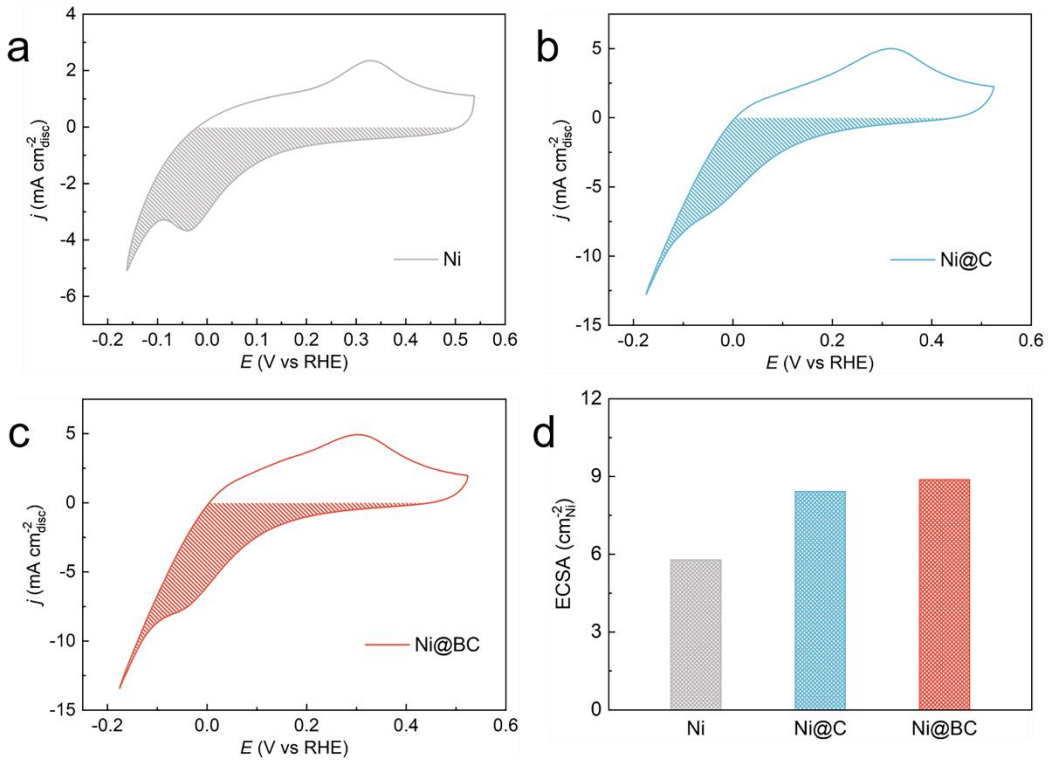

Figure S23. CVs of (a) Ni, (b) Ni@C, and (c) Ni@BC in Ar-saturated 0.1 M KOH at a scan rate of 50 mV s^{-1}. (d) ECSAs of these three catalysts.

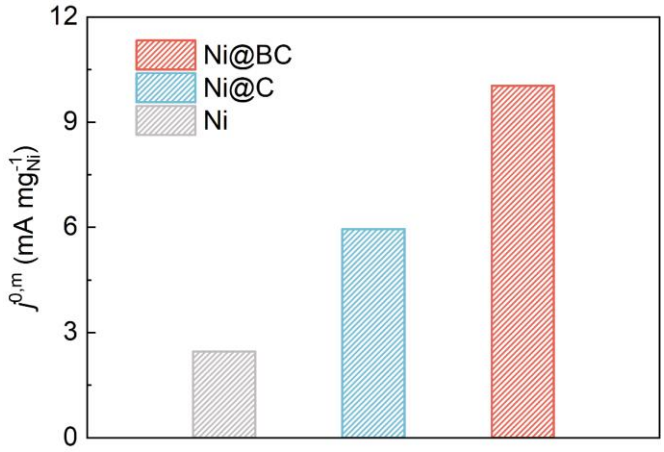

Figure S24. Comparison of the metal mass-normalized exchange current densities of Ni, Ni@C and Ni@BC.

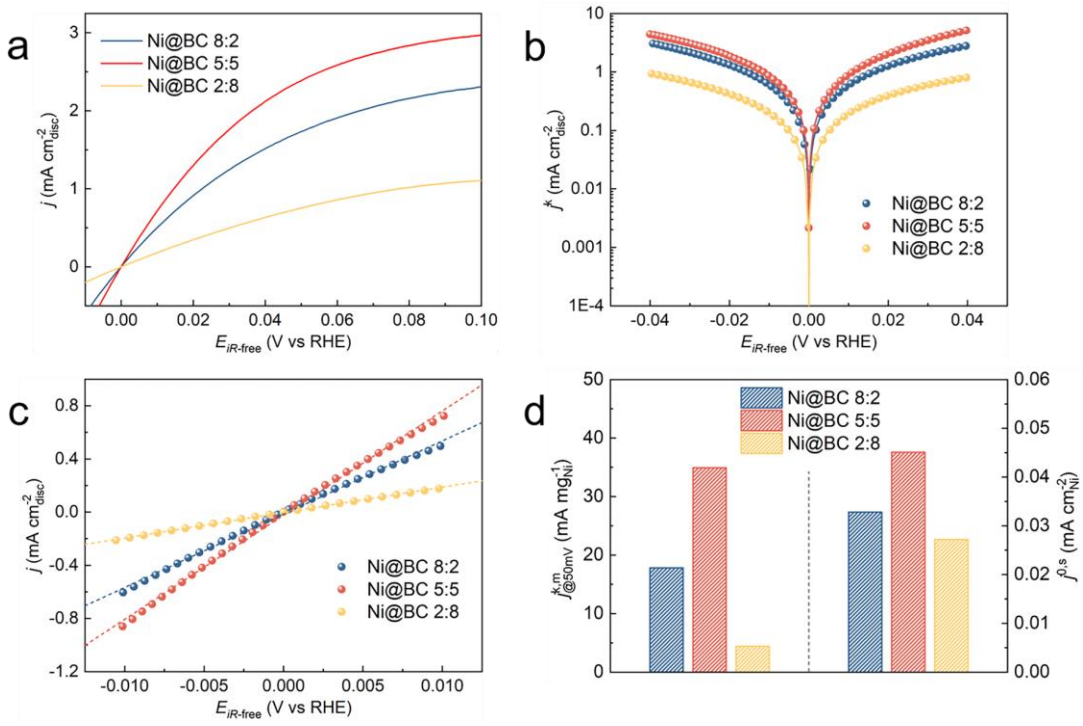

Figure S25. (a) HOR polarization curves of Ni@BC 8:2, Ni@BC 5:5 and Ni@BC 2:8 in H_2-saturated 0.1 M KOH solution at the rotating speed of 2500 rpm. (b) Tafel plots derived from HOR polarization curves of Ni@BC 8:2, Ni@BC 5:5 and Ni@BC 2:8 normalized kinetic current densities (j^k) via the Butler-Volmer fittings. (c) Linear fitting curves in the micro-polarization region. (d) Comparison of the metal mass-normalized

kinetics current densities ($j^{k,m}$) at an overpotential of 50 mV and the ECSA-normalized exchange current densities ($j^{0,s}$) of the three catalysts.

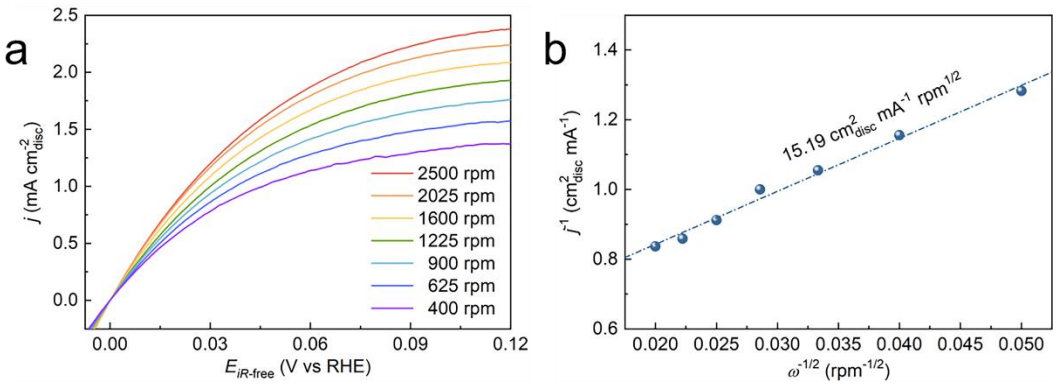

Figure S26. (a) HOR polarization curves of Ni@BC 8:2 in H_2-saturated 0.1 M KOH with a scan rate of 5 mV s^{-1} at the rotating speeds varied from 2500 to 400 rpm. (b) Koutecky–Levich plot obtained from (a) at an overpotential of 30 mV.

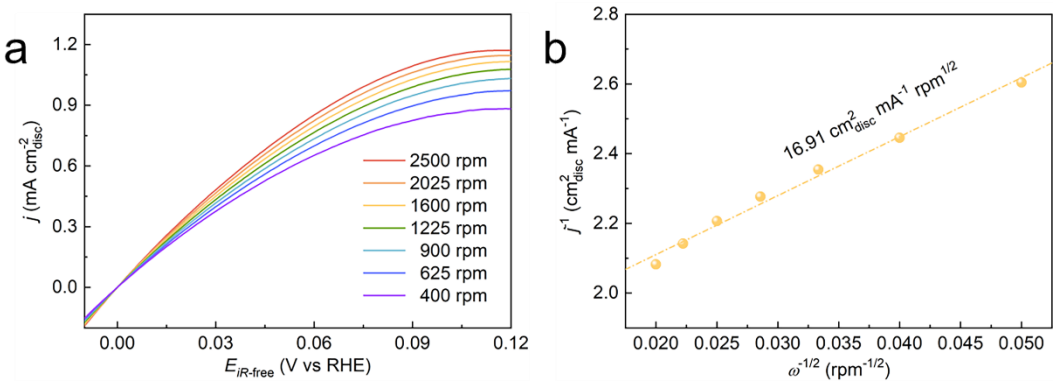

Figure S27. (a) HOR polarization curves of Ni@BC 2:8 in H_2-saturated 0.1 M KOH with a scan rate of 5 mV s^{-1} at the rotating speeds varied from 2500 to 400 rpm. (b) Koutecky–Levich plot obtained from (a) at an overpotential of 30 mV.

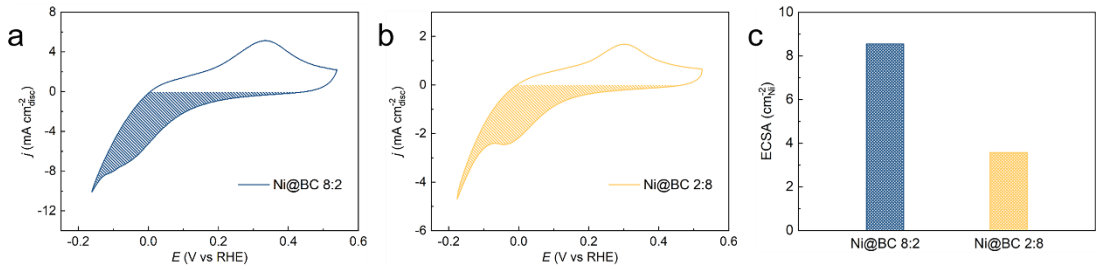

Figure S28. CVs of (a) Ni@BC 8:2 and (b) Ni@BC 2:8 in Ar-saturated 0.1 M KOH at a scan rate of 50 mV s^{-1}. (d) ECSAs of these two catalysts.

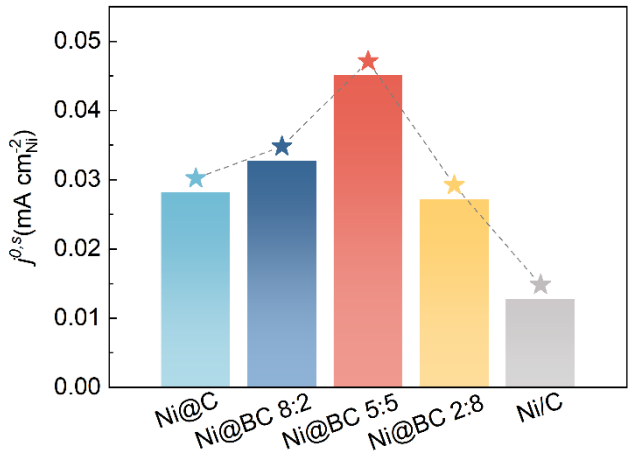

Figure S29. Comparison of the ECSA-normalized exchange current densities ($j^{0,s}$) of Ni, Ni@C, Ni@BC 8:2, Ni@BC 5:5 and Ni@BC 2:8.

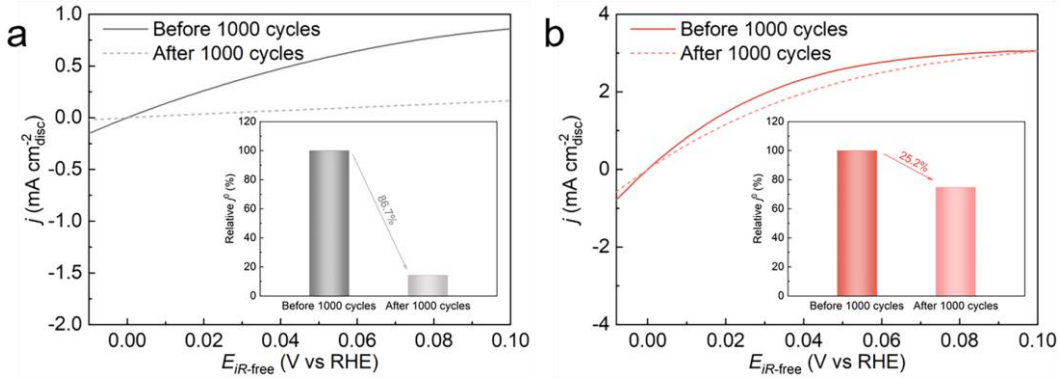

Figure S30. HOR polarization curves for Ni (a) and Ni@BC (b) in H_2-saturated 0.1 M

KOH before and after 1000 cycles. The inset bar plot is a comparison of j^0 before and after 1000 cycles.

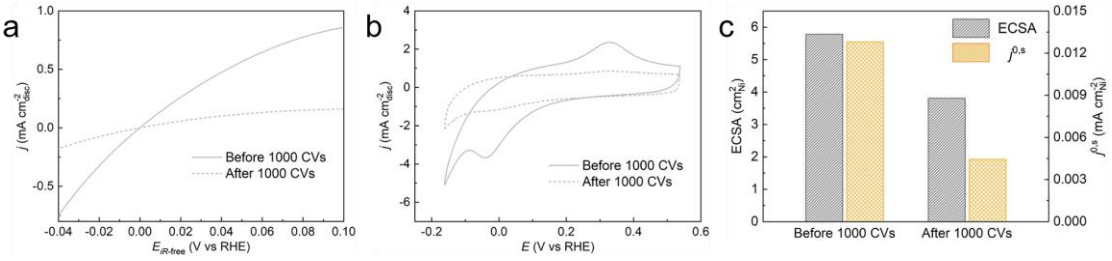

Figure S31. (a) CV curves in Ar-saturated 0.1 M KOH at a scan rate of 50 mV s^{-1}, (b) HOR polarization curves in H_2-saturated 0.1 M KOH with a scan rate of 5 mV s^{-1} at a rotating rate of 2500 rpm, and (c) ECSA and specific activities of Ni@BC before and after 1000 CV cycles.

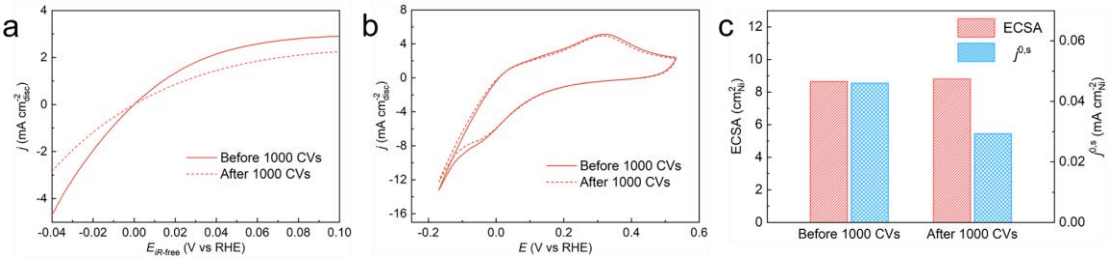

Figure S32. (a) CV curves in Ar-saturated 0.1 M KOH at a scan rate of 50 mV s^{-1}, (b) HOR polarization curves in H_2-saturated 0.1 M KOH with a scan rate of 5 mV s^{-1} at a rotating rate of 2500 rpm, and (c) ECSA and specific activities of Ni@BC before and after 1000 CV cycles.

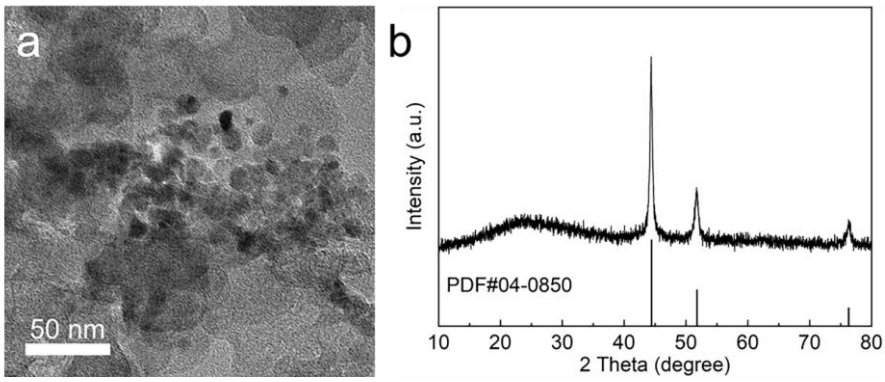

Figure S33. TEM image and XRD patterns of Ni@BC after accelerated durability test.

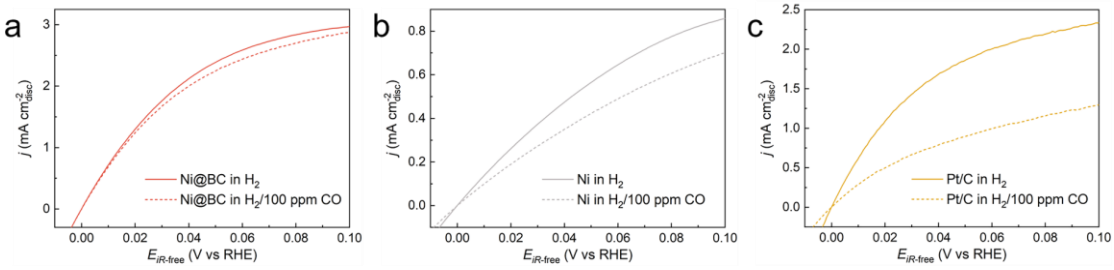

Figure S34. HOR polarization curves on (a) Ni@BC, (b) Ni and (c) commercial Pt/C catalyst in pure H_2 (solid lines), and H_2 with 100 ppm CO (dash lines) in 0.1 M KOH electrolyte, with rotating speed of 2500 rpm for Ni@BC and Ni catalysts, and 1600 rpm for Pt/C.

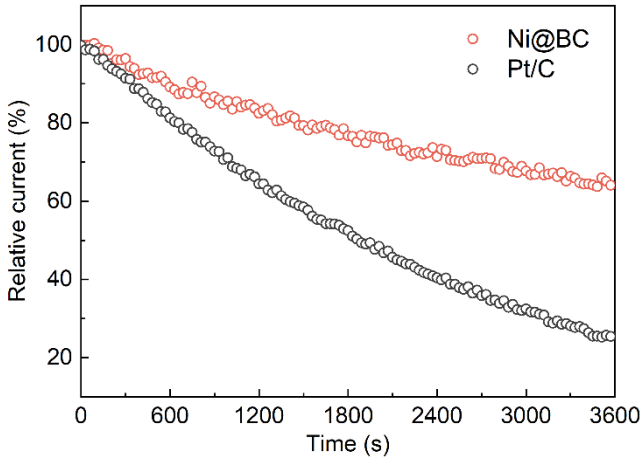

Figure S35. Chronoamperometry curves of Ni@BC and Pt/C in 0.1 M KOH saturated

with H_2 (containing 100 ppm CO) measured at 0.05 V.

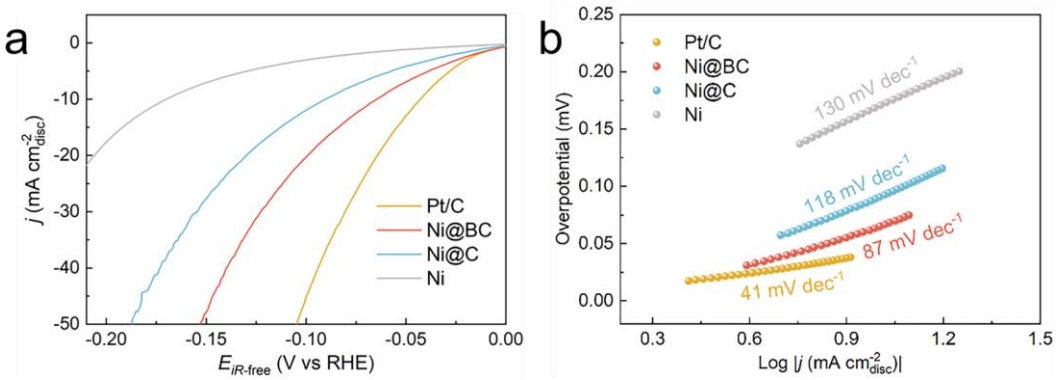

Figure S36. (a) HER polarization curves of Ni, Ni@C, Ni@BC and Pt/C in Ar-saturated 1 M KOH with a scan rate of 5 mV s^{-1} at a rotating rate of 1600 rpm. (b) Tafel slopes of catalysts deduced from (a).

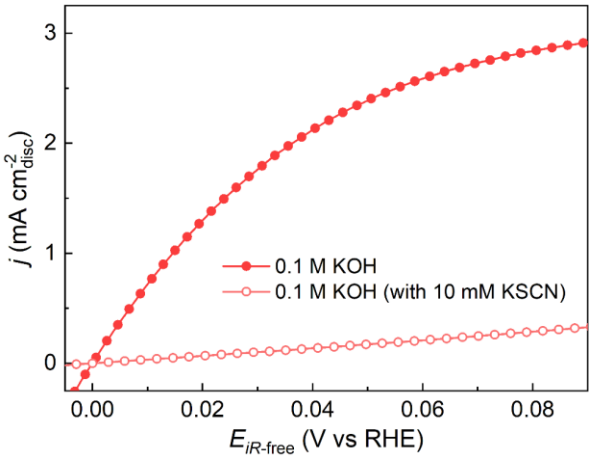

Figure S37. HOR polarization curves of Ni@BC with and without the addition of KSCN in 0.1 M KOH.

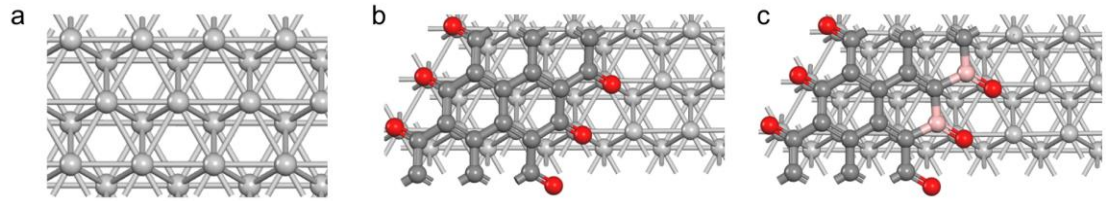

Figure S38. The theoretical models from the top view of pristine Ni (a), Ni@C (b), and Ni@BC (c), respectively. Ni, C, B, and O atoms are denoted by silver, dark gray, pink, and red spheres, respectively.

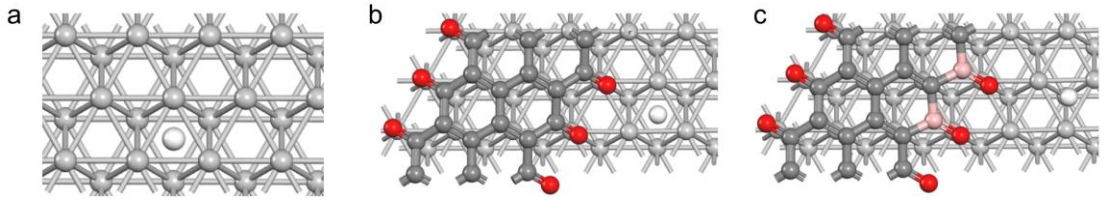

Figure S39. The theoretical models from the top view of adsorbed H^* on pristine Ni (a), Ni@C (b), and Ni@BC (c), respectively. Ni, C, B, O, and H atoms are denoted by silver, dark gray, pink, red, and white spheres, respectively.

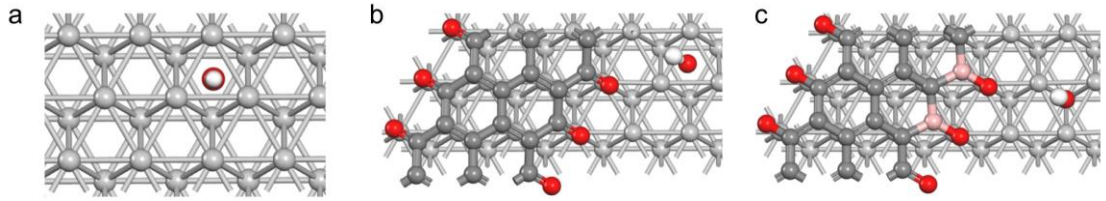

Figure S40. The theoretical models from the top view of adsorbed OH^* on pristine Ni (a), Ni@C (b), and Ni@BC (c), respectively. Ni, C, B, O, and H atoms are denoted by silver, dark gray, pink, red, and white spheres, respectively.

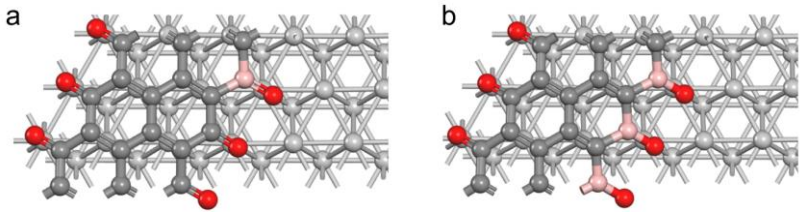

Figure S41. The theoretical models from the top view of Ni@B_sC (a) and Ni@B_rC (b), respectively. Ni, C, B, and O atoms are denoted by silver, dark gray, pink, and red spheres, respectively.

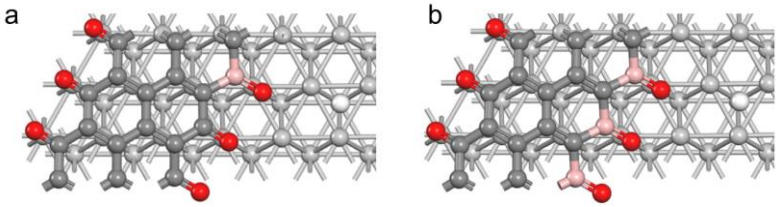

Figure S42. The theoretical models from the top view of adsorbed H^* on Ni@B_sC (a) and Ni@B_rC (b), respectively. Ni, C, B, O, and H atoms are denoted by silver, dark gray, pink, red, and white spheres, respectively.

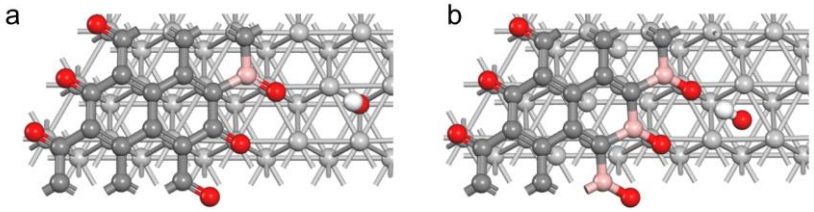

Figure S43. The theoretical models from the top view of adsorbed OH^* on Ni@B_sC (a) and Ni@B_rC (b), respectively. Ni, C, B, O, and H atoms are denoted by silver, dark gray, pink, red, and white spheres, respectively.

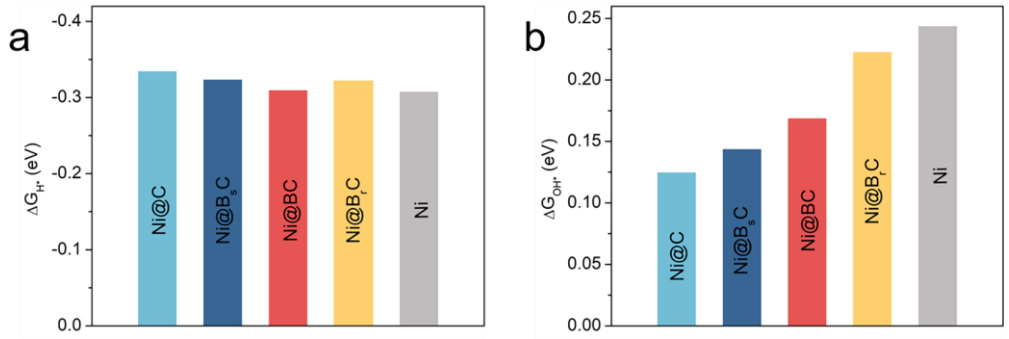

Figure S44. (a)The calculated Gibbs free energy of adsorbed H^* (ΔG_{H^*}) values of pristine Ni, Ni@C, Ni@B_sC, Ni@BC, and Ni@B_rC. (b)The calculated Gibbs free energy of adsorbed OH^* (ΔG_{OH^*}) values of pristine Ni, Ni@C, Ni@B_sC, Ni@BC, and Ni@B_rC.

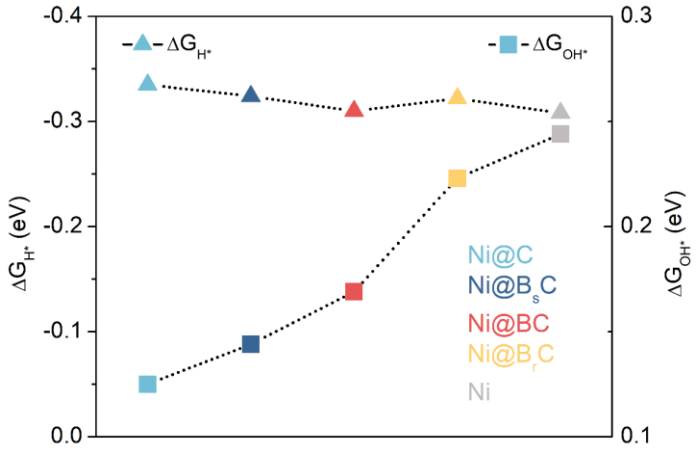

Figure S45. Calculated ΔG_{H^*} and ΔG_{OH^*} values of pristine Ni, Ni@C, Ni@B_sC, Ni@BC, and Ni@B_rC.

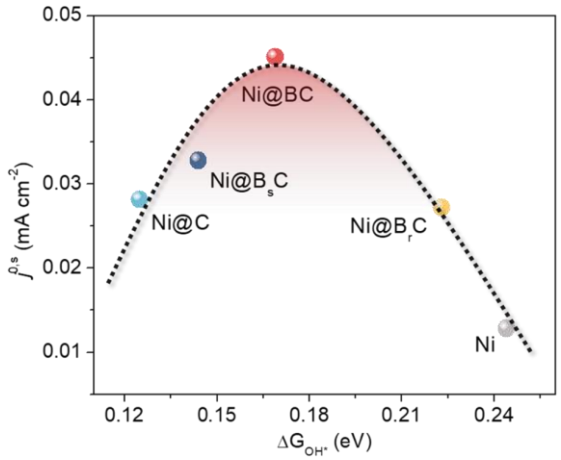

Figure S46. Volcano plot of the HOR intrinsic activity ($j^{0,s}$) as a function of the ΔG_{OH*} for pristine Ni, Ni@C, Ni@B_sC, Ni@BC, and Ni@B_rC catalysts.

Table S1. The atomic content of C and B determined by XPS.

Sample	C (atomic %)	B (atomic %)
Ni@C	69.33	/
Ni@B-C-8:2	62.04	1.07
Ni@B-C-5:5	38.94	3.26
Ni@B-C-2:8	26.99	11.2

Table S2. ICP-AES results of Ni@C, Ni@BC 8:2, Ni@BC 5:5 and Ni@BC 2:8.

Catalyst	Ni (wt%)	Loding on GC (mg_{Ni} cm^{-2})
Ni@C	84.07	0.206
Ni@BC 8:2	83.88	0.205
Ni@BC 5:5	83.00	0.203
Ni@BC 2:8	93.42	0.228

Table S3. Comparison of the HOR activity in 0.1 M KOH for catalysts in this work with reported benchmark Ni-based catalysts.

Sample	Temperature /K	Loading ($mg_{Ni}\ cm^{-2}$)	$j^{0,s}$ ($mA\ cm_{Ni}^{-2}$)	$j^{k,m}$@50mV ($mA\ mg_{Ni}^{-1}$)	Reference
Ni@BC	303	0.203	0.045	34.91	This work
Ni/N-CNT	r.t.	0.25	0.028	9.3	*Nat. Commun.*, 2016, **7**, 10141
CeO_2(r)-Ni/C-1	303	0.141	0.038	12.28	*Angew. Chem. Int. Ed.*, 2019, **58**, 14179-14183
Ni_3N/C	/	0.16	0.014	24.38	*Angew. Chem. Int. Ed.*, 2019, **58**, 7445-7449
Ni/NiO/C-700	298	0.16	0.026	5.0	*Angew. Chem. Int. Ed.*, 2019, **58**, 10644-10649
CoNiMo	293	/	0.015 (α=0.5) 0.007 (α=1.0)	/	*Energy Environ. Sci.*, 2014, **7**, 1719-1724
np-Ni_3N	298	0.16	/	29.75	*Energy Environ. Sci.*, 2019, **12**, 3522-3529
Ni_3@$(hBN)_1$/C -700NH_3	/	0.25	0.023	/	*Chem. Sci.*, 2017, **8**, 5728-5734

Ni/SC	303	0.138	0.040	8.6	*J. Mater. Chem. A*, 2019, **7**, 10936-10941
NiB-300	303	0.142	0.025	24.7	*Chem. Sci.*, 2020, **11**, 12118-12123
Ni/Ni_3N-C	303 (±0.1)	0.166	0.036	12.176	*Adv. Funct. Mater.*, 2021, **31**, 2106156
Ni@NC -PEI-XC	/	0.255	0.038	24.4	*ACS Catal.*, 2021, **11**, 7422-7428
Ni_3C/C-350	/	0.2	0.031	13.6	*J. Mater. Chem. A*, 2021, **9**, 26323-26329
hcp/fcc-Ni-C	303	0.306	0.03088	12.28	*ACS Sustainable Chem. Eng.*, 2022, **10**, 3682-3689
Ni@C-500℃	303	0.1	0.032	/	*ACS Appl. Mater. Interfaces*, 2020, **12**, 31575-31581
$Ni_{100}Au_1$/C-EA	/	0.255	0.0473	17.9	*Chem. Eng. J.*, 2023, **464**, 142692
Ni_3N-r	/	0.32	0.038	40.69	*Angew. Chem. Int. Ed.*, 2022, **61**, e202206588
$Ni_{90}Fe_{10}$-C-500	298	0.197	0.048	11.0	*Eur. J. Inorg. Chem.*, 2022, e202200242

Ni/V_2O_3	/	0.175	0.038	42.1	*Angew. Chem. Int. Ed.*, 2023, **62**, e202217275
$Ni\text{-}H_2\text{-}2\%$	/	0.14	0.028	50.4	*Angew. Chem. Int. Ed.*, 2020, **59**, 10797-10801
$Ni_{5.2}WCu_{2.2}$	298	9.2	0.014	2.55	*Nat. Commun.*, 2021, **12**, 2686

References

1. Z. Zhuang, S. A. Giles, J. Zheng, G. R. Jenness, S. Caratzoulas, D. G. Vlachos and Y. Yan, *Nat. Commun.*, 2016, **7**, 10141.

2. W. Sheng, H. A. Gasteiger and Y. Shao-Horn, *J. Electrochem. Soc.*, 2010, **157**, B1529-B1536.

3. T. Tang, X. Liu, X. Luo, Z. Xue, H. Pan, J. Fu, Z. Yao, Z. Jiang, Z. Lyu, L. Zheng, D. Su, J. Zhang, L. Zhang and J. Hu, *J. Am. Chem. Soc.*, 2023, **145**, 13805-13815.

4. J. P. Perdew, K. Burke and M. Ernzerhof, *Phys. Rev. Lett.*, 1996, **77**, 3865-3868.

5. D. Vanderbilt, *Phys. Rev. B*, 1990, **41**, 7892-7895.

6. M. Methfessel and A. T. Paxton, *Phys. Rev. B*, 1989, **40**, 3616-3621.

7. J. Rossmeisl, A. Logadottir and J. K. Nørskov, *Chem. Phys.*, 2005, **319**, 178-184.

8. J. K. Nørskov, J. Rossmeisl, A. Logadottir, L. Lindqvist, J. R. Kitchin, T. Bligaard and H. J. Jónsson, *Phys. Chem. B*, 2004, **108**, 17886-17892.